Journal of Structural Geology, Vol. 11, No. 7, pp. 879 to 893, 1989
Printed in Great Britain

0191-8141/89 $03.00 + 0.00

The relationship between slickenside surfaces in fine-grained quartz and the seismic cycle

WILLIAM L. POWER* and TERRY E. TULLIS

Department of Geological Sciences, Brown University, Providence, RI 02912, U.S.A.

(*Received* 12 *December* 1988; *accepted in revised form* 14 *April* 1989)

Abstract—Well polished or reflective fault surfaces, with or without linear striae indicating the sliding direction, are commonly referred to as slickensides. This study examines the development of slickensides which are now exposed along the surface trace of a large, seismically active normal fault zone in Dixie Valley, Nevada, U.S.A. Geologic and mineralogic constraints indicate the slickenside surfaces formed at depths of less than 2 km and temperatures less than 270°C. The slickenside surface material is composed of greater than 98% quartz, with less than 2% kaolinite and iron oxide. Transmission electron microscope (TEM) observations reveal that the slickenside surface material has an extremely fine yet variable grain size (0.01–1 μm), and an unusual, non-equilibrium texture characterized by irregular grain boundaries and low dislocation density. Angular fragments in the cataclasite to either side of the slickensides provide clear evidence of cataclasis. Crystallographic preferred orientation in the slickenside surface material indicates that non-brittle, continuous deformation occurred within 0.1–10 mm of the fault surfaces in many areas. Non-brittle, continuous deformation must have alternated with cataclasis, because some fragments in the cataclasite have strong preferred orientations. We suggest that in the Dixie Valley slickensides, continuous deformation and the development of crystallographic preferred orientations occurred at relatively low strain rates during the interseismic period, while cataclasis occurred at higher strain rates associated with seismic events. The wide range of strain rates occurring within a fault zone during the earthquake cycle may be an essential element in the formation of fine-grained, glassy slickensides, both at Dixie Valley, Nevada, and many other areas.

INTRODUCTION

SHINY, reflective fault surfaces often termed slickensides are common in many faulting environments, but have received relatively little study (Tjia 1968, Means 1987, Petit 1987). Following Fleuty (1975) and Means (1987) we refer to fault surfaces as slickensides, as distinct from slip-parallel striae found on many, but not all, fault surfaces. Slickensides form through a wide variety of mechanisms, including: (1) frictional wear and surface polishing (Avakian 1986, Hancock & Barka 1987); (2) pressure-solution slip leading to the formation of surfaces covered by felted mats of fibrous crystals (Durney & Ramsay 1973, Elliott 1976); (3) streaking or trailing of lightly cemented gouge material (Tjia 1968, Engelder 1974); (4) strain alignment of clay particles during expansion and contraction in clay soils (Gray & Nickelsen 1989); and (5) plastic yielding and strain alignment of layer silicates prior to the development of discontinuous faults (Will & Wilson 1989). Slickenside features have been widely utilized to determine the direction and, in some cases, the sense of slip on fault surfaces. This information is useful because it allows one to infer the strain history of large rock masses (Wojtal 1986, Hancock & Barka 1987) or, by inference, the stress state that caused faulting and deformation (Angelier 1979, Angelier *et al.* 1985, Zoback 1989).

Additionally, the study of slickensides has the potential to provide insights into the grain-scale deformation mechanisms that are active along frictional rock surfaces, contributing to the understanding of the mechanical properties of fault zones and their evolution. One particularly important reason for studying the surfaces is that certain slickenside types or features may be indicative of different phases of the earthquake cycle. The earthquake cycle is often divided into four phases: an interseismic phase (quiescent period between earthquakes), a pre-seismic phase (foreshocks and accelerating creep), a co-seismic phase (rapid slip during earthquakes) and, finally, a post-seismic phase (aftershocks and decelerating creep). Some faults may not experience all four stages. Some examples of fault surface features that have been attributed to the seismic phase of the earthquake cycle include carrot-shaped asperity grooves (Engelder 1974), pseudotachylytes or friction melts (Sibson 1975) and crescent-shaped tension fractures (Petit 1987). Fibrous pressure-solution slip slickensides such as those described by Durney & Ramsay (1973) and Elliott (1976) probably develop during slow aseismic creep rather than during seismic events. The possibility of finding other features which can be directly linked to seismically or geodetically observed aspects of fault behavior is great, and should be pursued.

One important implication of the earthquake cycle for the development of fault zone materials is that an extremely wide range of strain rates will prevail along faults that experience seismic slip events (Sibson 1977). Relative slip rates along faults range from velocities as high as 1–2 m s^{-1} during seismic events (Brune 1976) to 1–30 mm yr^{-1} during steady, aseismic shearing (Thatcher 1979, Burford & Harsh 1980, Sibson 1983). If

* Present address: CSIRO Division of Geomechanics, P.O. Box 54, Mt. Waverley, Victoria 3149, Australia.

deformation during seismic faulting events is confined to relatively thin and discrete principal slip surfaces, as is often observed (Sibson 1986a), strain rates as high as 10^2–10^4 s^{-1} might occur in the fault zone. In contrast, strain rates more typical of deformation during the interseismic period probably range from 10^{-10} to 10^{-15} s^{-1}, or perhaps less (Sibson 1977, Pfiffner & Ramsay 1982).

Major fault zones with large displacements and significant components of dip-slip provide the opportunity to directly observe the effects of faulting on materials under non-surface conditions, because slip on the fault surfaces 'exhumes' materials from depth. In this study we describe and interpret textural and mineralogical features of exhumed normal fault surfaces from Dixie Valley, Nevada, U.S.A. The slickenside surfaces we describe, however, are not unique to the Dixie Valley area; we infer that many other glassy slickensides composed of fine-grained quartz formed in much the same way as those at Dixie Valley. We conclude by offering some preliminary inferences concerning the relationship of specific slickenside features to the earthquake cycle.

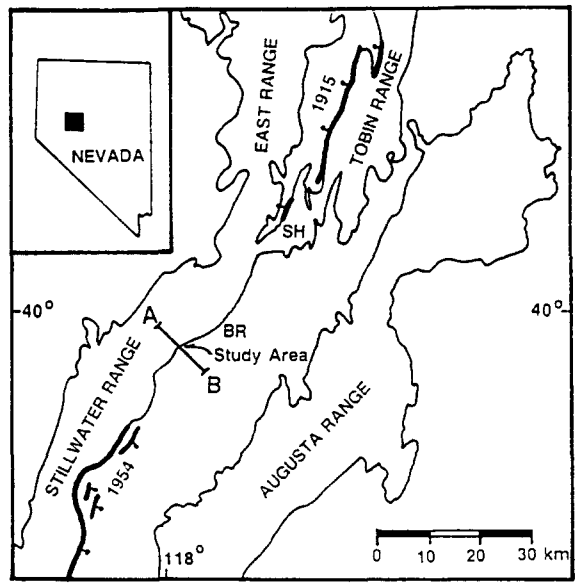

Fig. 1. Location map showing the Stillwater seismic gap and the slickenside study area. The line labeled A–B shows the location of the cross-section shown as Fig. 2. Surface ruptures of the 1915 and 1954 earthquakes are shown as heavy lines. Abbreviations as follows: SH—Sou Hills, BR—Boyer Ranch. Total normal slip on the Stillwater range-front fault is about 0.3 km in the Sou Hills (Fonseca 1988) and 3 km at Boyer Ranch (Okaya & Thompson 1985). Total normal slip on the Stillwater fault at the study area is 3–6 km.

GEOLOGIC SETTING

Before describing the slickenside surfaces, we briefly review the geologic history of the Dixie Valley area (Fig. 1). More extensive information can be found in studies by Page (1965), Anderson *et al.* (1983), Wallace & Whitney (1984) and Okaya & Thompson (1985). The fault zone we investigated lies within an area termed the "Stillwater seismic gap" by Wallace & Whitney (1984), because major historic earthquakes occurred immediately to the north in Pleasant Valley in 1915, and immediately to the south in southern Dixie Valley in 1954. Fault scarps within the Stillwater seismic gap (Wallace & Whitney 1984), and offset shorelines of prehistoric lakes (Thompson & Burke 1973) provide evidence of displacement within the last 12,000 years. The Stillwater seismic gap is relatively quiet in terms of microearthquake activity, but areas to the north and south still show elevated levels of microearthquakes (Dozer 1986). It is clear that earthquakes will occur in the study area in the future, and that seismic faulting played an important part in the development of the fault zone materials now exposed in Dixie Valley.

For the purposes of this study, rock materials in the region are divided into three groups (Fig. 2): 'basement' rocks of Mesozoic age; volcanic and sedimentary rocks of early Tertiary age, which pre-date the development of the fault zone; and alluvial and lacustrine sediments of late Tertiary and Pleistocene age, which accumulated concurrently with faulting. The basement rocks consist of a wide variety of variably metamorphosed, primarily Cretaceous age rocks, including pelites, granodiorites and gabbros (Page 1965, Okaya & Thompson 1985).

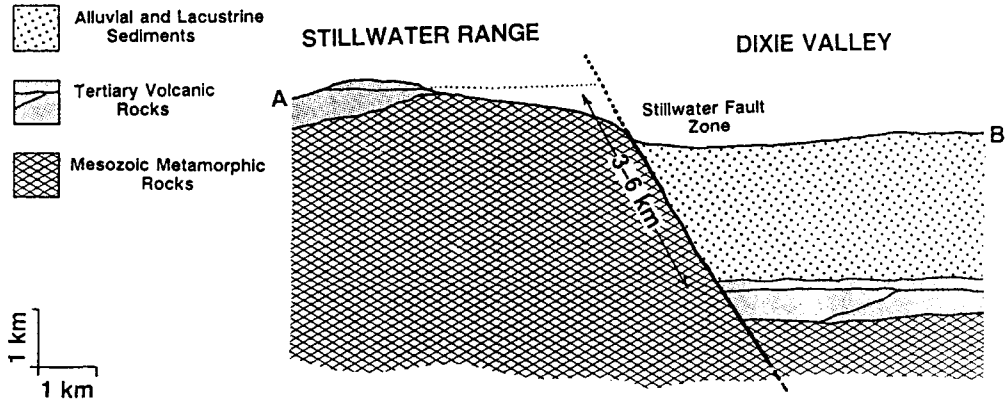

Fig. 2. Cross-section showing the geometry of the Stillwater fault zone in the study area. Total normal slip across the Stillwater fault can be estimated from the offset of the youngest part of the Tertiary section, a widespread and flat-lying basaltic flow which outcrops at the crest of the Stillwater range and underlies the syntectonic valley fill of alluvial and lacustrine sediments. Location of this section is shown on Fig. 1 as line A–B.

The basement rocks are unconformably overlain by a variety of Tertiary age sedimentary and volcanic rocks which pre-date the development of steep normal faults in the Dixie Valley area (Riehle *et al.* 1972, Hastings 1979). The Tertiary sequence is capped by an 11–17 Ma old unit of basaltic volcanic flows and pyroclastics (Hastings 1979, Fonseca 1988).

Late Cenozoic extension of the Dixie Valley area disrupted the Mesozoic and early Tertiary age rocks, resulting in the development of a major, range-front fault zone on the east side of the Stillwater Range. We refer to this fault as the Stillwater fault, following Wallace & Whitney (1984) and Fonseca (1988). The surface trace of the Stillwater fault at the current level of exposure is characterized by a variety of fault rocks that originally formed under different conditions. In most places there is no single fault surface. Rather, the fault zone consists either of a uniform clay gouge zone, or of many discrete surfaces separating fault bounded horses of cataclasite, breccia, or variably deformed and fractured wallrocks. In scattered locations along the fault trace, slickenside surfaces composed almost entirely of fine-grained quartz are present.

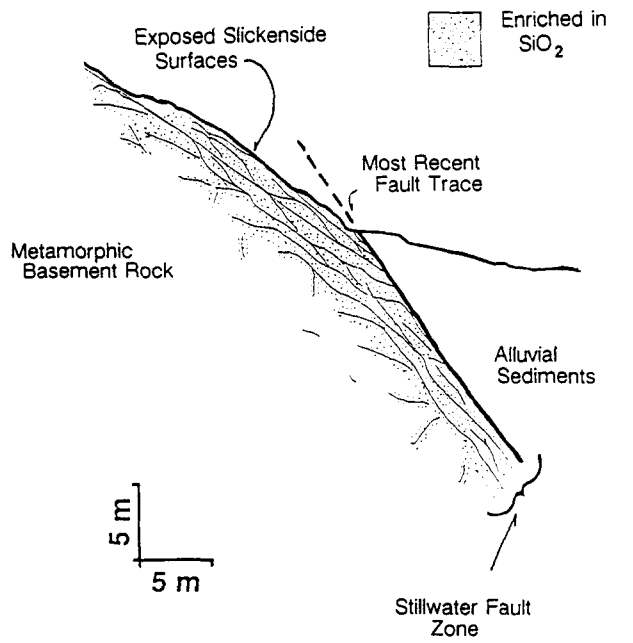

Fig. 3. Schematic outcrop scale cross-section illustrating the details of the slickenside study locality. In the study area, the fault zone juxtaposes Mesozoic metamorphic rock against alluvial sediments. The most recently active fault surface occurs at the base of the exposure of metamorphic rock. The slickenside surfaces are found in the footwall block, in areas that have been strongly enriched in quartz by precipitation from hydrothermal fluids.

Slickenside locality

This study concentrates on a unique part of the fault zone where slickenside surfaces which developed in fine-grained, hydrothermal quartz are well exposed (Fig. 1—39.95° N. Lat., 117.95° W. Long.). In the study area, the most recent trace of the Stillwater fault juxtaposes alluvial sediments against metamorphosed Jurassic age gabbroic rocks (Fig. 3). Although the host rock for the slickenside surfaces is metamorphosed gabbro, the slickenside surfaces occur only in areas that have experienced extensive enrichment in silica due to the passage of hydrothermal fluids. The exposure of shiny, reflective fault surfaces is approximately 100 m long parallel to the strike of the fault zone. The largest exposures of a single surface are about 25 m^2. Other, similar slickenside surfaces can be found along the Dixie Valley fault zone, but none are as large as those described in this study.

We estimate that total normal slip on the Stillwater fault zone at the slickenside locality is 3–6 km. Gravity studies, combined with reflection seismology studies (Okaya & Thompson 1985) and unpublished well data (reviewed by Fonseca 1988), indicate that Dixie Valley is filled with alluvial and lacustrine sediments floored by the same sequence of early Tertiary volcanic rocks found on the top of the Stillwater Range (Fig. 2). Normal slip, estimated from the separation of the Tertiary volcanic sequence, varies from about 300 m in the Sou Hills (Fig. 1—approximately 23 km north of the study area) to 3 km at Boyer Ranch (approximately 8 km north of the study area). Because total normal slip varies along the fault zone, and generally increases southwards, total normal slip at the study area is probably between 3 and 6 km.

We conclude that the slickenside surfaces formed at a depth of less than 2 km because: (1) the current exposure level of the footwall materials is approximately 1 km below the base of the Tertiary volcanic sequence; (2) the total thickness of the Tertiary volcanic sequence is approximately 1 km; and (3) normal faults developed in the Dixie Valley area after the deposition of the Tertiary volcanic sequence (Fig. 2). Thermal gradients of 20–45°C km^{-1} are typical of the Basin and Range Province (Lachenbruch & Sass 1977), but ongoing geothermal energy investigations in the Dixie Valley region indicate that gradients as high as 150–200°C km^{-1} may prevail at least temporarily near the Stillwater fault zone (Parchman & Knox 1981). This range of thermal gradients suggests that the slickenside surfaces developed at temperatures between 50 and 400°C. Test wells drilled to depths of 3 km encountered temperatures of approximately 200°C (Denton *et al.* 1980), in general concurrence with this conclusion. The presence of the assemblage kaolinite + quartz in the slickenside surface material (discussed below) provides independent evidence that temperatures were below 270°C during slickenside formation.

SLICKENSIDE SURFACES

Surface roughness and striation features

The slickenside surfaces in the study area may be divided into a three-fold classification based on surface morphology. To illustrate the range of roughness of the fault surfaces, we show 0.5 m profiles from each of three surfaces (Fig. 4). These profiles were measured parallel

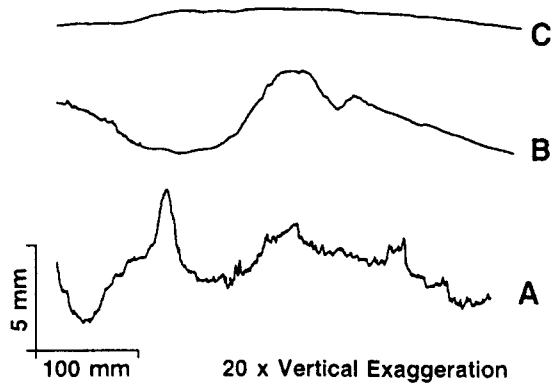

Fig. 4. Surface profiles of typical slickenside surfaces. The surfaces have a variety of roughnesses, ranging from moderately rough (A), through intermediate (B), to very smooth (C). The smoothest surfaces have the largest exposure areas.

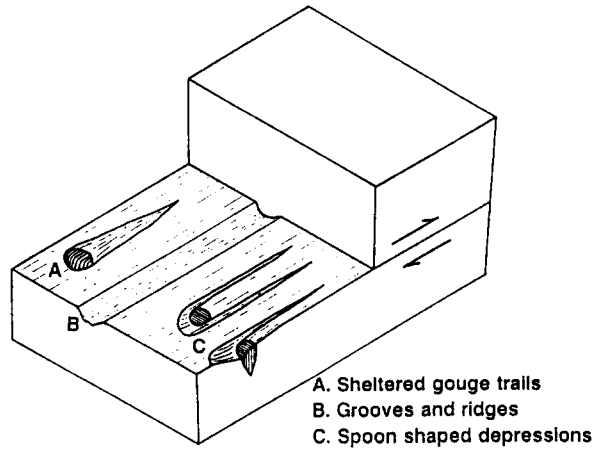

Fig. 5. Surface features of Dixie Valley slickenside surfaces. Features labeled are as follows: hard asperity, protruding above the surface, with lightly cemented gouge material on its lee side (A); interlocking ridges and grooves (B); spoon shaped depressions which form around small hard particles (C).

to the slip direction, using equipment and techniques described by Power *et al.* (1987, 1988). The Dixie Valley surfaces range from moderately rough (A—Fig. 4), to intermediate (B—Fig. 4) and finally to very smooth (C—Fig. 4). As can be deduced from the surface profiles, the maximum amplitude to wavelength ratio of each surface profile varies from about 1/100 for the roughest surfaces to about 1/500 for the smoothest surfaces. The surfaces have a generally self-similar geometry. This means that surface profiles observed at an enlarged or reduced scale appear statistically similar (Power *et al.* 1988).

On the roughest surfaces (A—Fig. 4) much of the roughness is the result of small, hard clasts in the footwall surface (A—Fig. 5). Curiously, in the area we examined, all the clasts are in the footwall surface, while matching depressions or indentations are present in the hangingwall surface. The roughest surfaces are generally small in areal extent, and do not form prominent weathering or parting surfaces.

The intermediate roughness surfaces (B—Fig. 4) have a ridge and groove geometry (B—Fig. 5). Ridges from one surface match grooves from the opposing surface. Means (1987) described geometrically similar surfaces. The grooves and ridges decrease in height or depth along the slip direction gradually, rather than beginning or ending at discrete asperities or hard clasts. Most ridges or grooves are 10–100 times as long in the direction parallel to slip as in the direction perpendicular to slip.

The smoothest and most reflective slickensides (C—Fig. 4) have the thickest accumulations of fine-grained quartz to either side of their surfaces. These surfaces often have spoon-shaped depressions formed by localized deformation around a hard clast or asperity, which are commonly composed of either single crystals of quartz, or of fragments of well indurated but reworked cataclasite (C—Fig. 5). For the smoothest surfaces, it was not possible to examine both the hangingwall and footwall surfaces to determine how well the surfaces match one another. The smoothest fault surfaces form the largest, most continuous exposures, probably because their flatness allows large blocks of the hangingwall to part easily from the footwall.

The difference in roughness of the various subparallel surfaces is difficult to explain. Although one tempting explanation is that rougher surfaces have less total displacement than the smoother surfaces, this possibility cannot be evaluated because it is difficult to estimate the total displacement for individual surfaces. Slip on most of the surfaces must be at least 1 m, based on color contrasts in the cataclasite to either side of many of the surfaces. Slip on any one surface must also be well under 3–6 km, because that is the total slip across the Stillwater fault zone. Another possible explanation for the difference in surface character is that the surfaces formed under different conditions of depth, confining pressure, temperature, strain rate or chemical environment.

Mineralogy, composition and temperature

The slickenside surfaces occur within a 1–10 m thick zone of cataclasite which has been considerably enriched in quartz relative to the gabbroic wallrock. The enrichment in silica is most extreme closest to the fault surfaces, and probably results from the passage of hydrothermal fluids through the fault zone. The fine-grained material within 1–10 mm of the fault surfaces consists of greater than 98% quartz. Energy dispersive X-ray composition determinations made with scanning and transmission electron microscopes reveal that the only common elements in the fine-grained slickenside material are Si, Fe and Al. The iron occurs in scattered iron oxide particles, particularly within 10–20 μm of the sliding surfaces. The aluminium occurs in fine-grained (0.01–0.1 μm) kaolinite flakes (Fig. 6a).

The slickenside surfaces must have formed at temperatures less than 270°C because both kaolinite and quartz are present in the fine-grained surface material. Kaolinite and quartz react to form pyrophyllite and water at temperatures of approximately 270°C over a wide range of pressures, under conditions where the

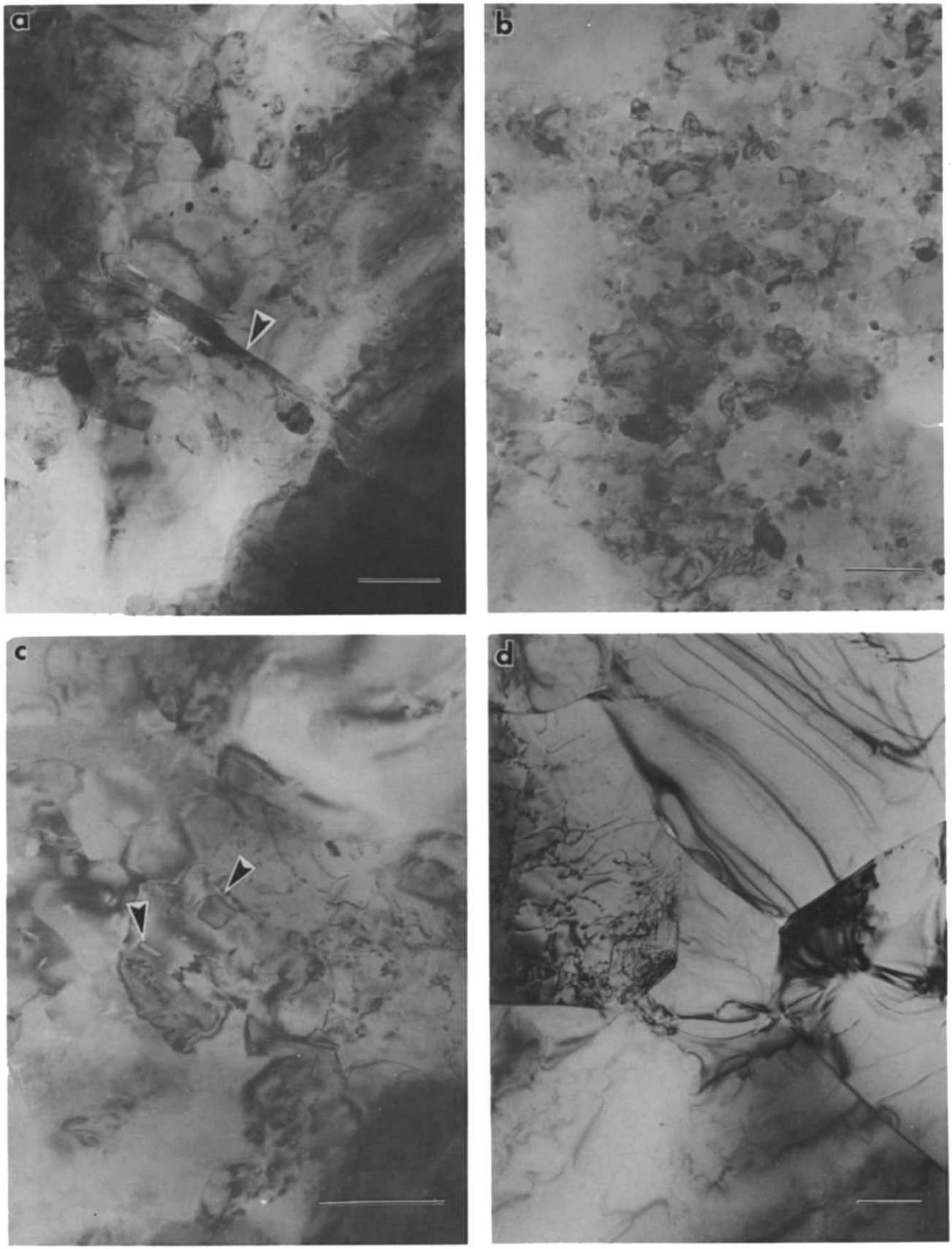

Fig. 6. Transmission electron microscope (TEM) micrographs of textural features found in fine-grained quartz. All scale bars 0.5 μm. (a) Slickenside surface material. Note kaolinite grain (arrow) surrounded by fine-grained quartz. This kaolinite grain is particularly large; most range in size from 0.01 to 0.1 μm. (b) Typical view of the slickenside surface material, which has a wide range of grain sizes (0.01–0.1 μm). (c) Smaller grains within the slickenside surface material (arrows) are often completely enclosed within larger grains, a configuration of high surface energy. (d) Micrographs of a fine-grained novaculite (not from the Stillwater fault zone) which was experimentally deformed in the dislocation creep field. In contrast to the slickenside material, the novaculite has a narrow range of grain sizes (1–5 μm), polygonal grain shapes and straight grain boundaries.

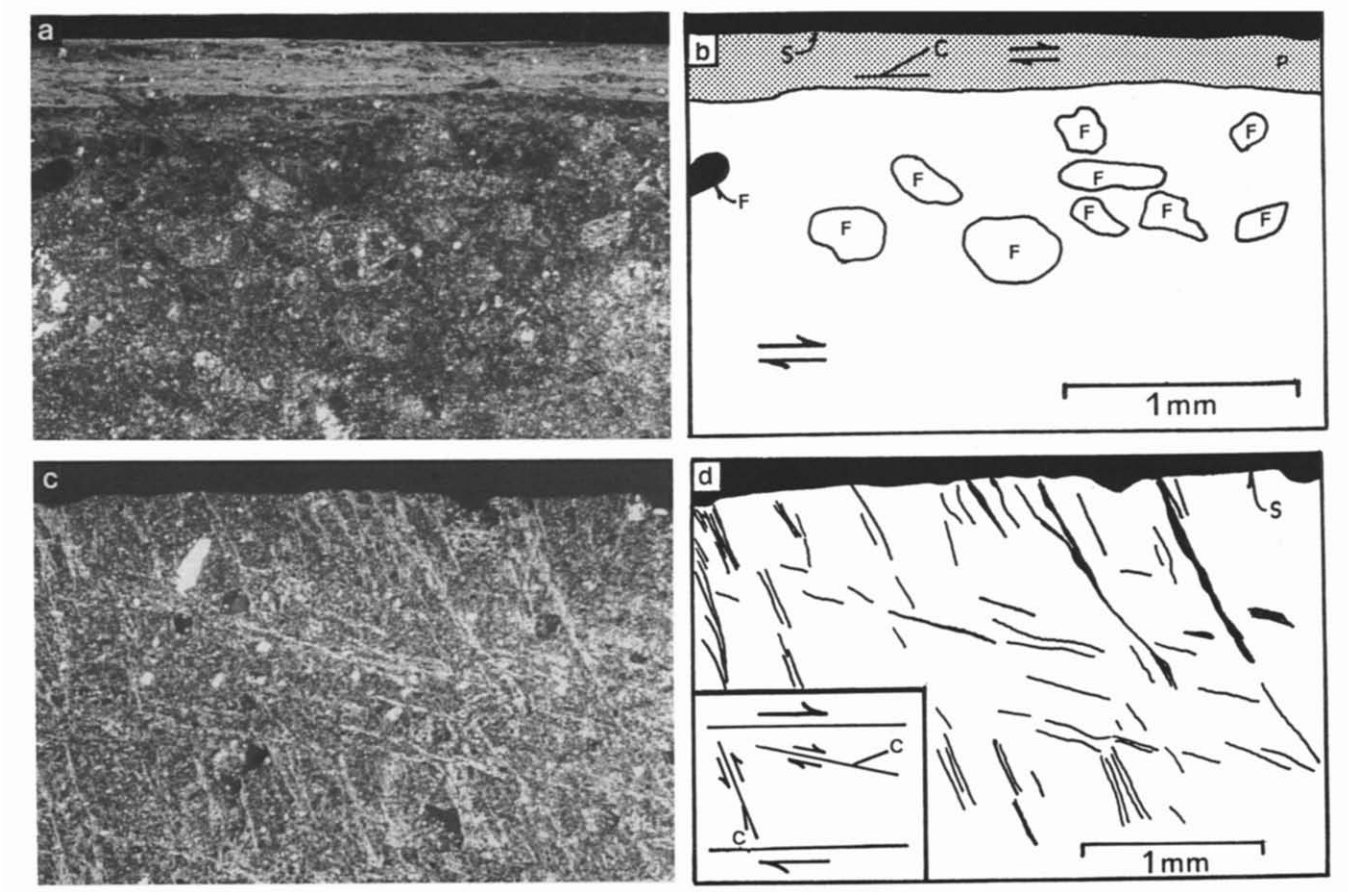

Fig. 7. Optical photomicrographs illustrating crystallographic preferred orientation in fine-grained quartz along the fault surfaces. The photomicrographs were taken with crossed polarizers; areas of the samples with preferred orientation appear either lighter or darker than the background. (a) A simple, 0.2 mm thick, preferred orientation zone with essentially one orientation of quartz *c*-axes. (b) Schematic view of (a). The fault surface (S) is developed on/in an area of strong crystallographic preferred orientation (P—shaded). Quartz *c*-axes are inclined in the direction of shear. Fragments in the cataclasite (F) are visible beneath the zone of preferred orientation. (c) A more complex array of preferred orientation zones. (d) Schematic view of (c). The fault surface (S) is underlain by a zone of fine-grained quartz with an array of preferred orientation zones reminiscent of Riedel shear geometry (Logan *et al.* 1979). The position of the quartz *c*-axes within each preferred orientation zone is consistent with slip on each shear zone in the sense shown (inset), but there is no independent evidence that actual displacement occurred across either the steeply or shallowly inclined surfaces.

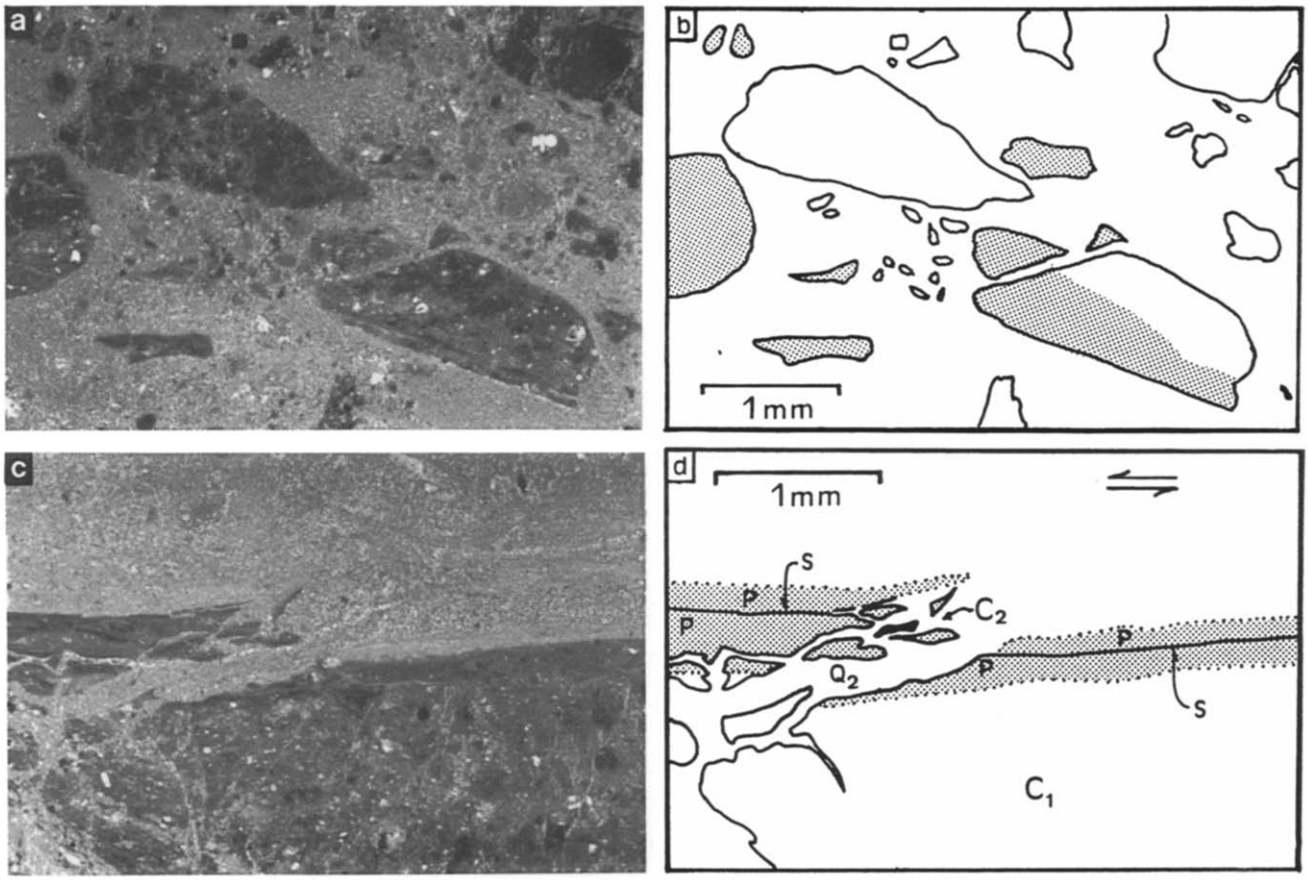

Fig. 9. Photomicrographs illustrating textural features of the cataclasite that forms the slickenside surfaces. (a) Cataclasite fragments cemented together with fine-grained hydrothermal quartz. (b) Schematic view of (a). Some fragments consist of earlier cataclasites which have crystallographic preferred orientation zones very similar to those shown in Fig. 7(a). Shaded areas have strong crystallographic preferred orientation. These textures indicate that conditions favorable for continuous, non-brittle deformation and the development of crystallographic preferred orientations alternated with conditions favorable for discontinuous cataclasis. (c) Well preserved textures along the fault surfaces indicate repetitive cycles of continuous and discontinuous deformation. (d) Schematic view of (c). An early cataclasite (C_1), truncated by a fault surface are the earliest textural features visible. Associated with the fault surface (S) are preferred orientation zones which are shown shaded (P). Preferred orientation developed in both the early cataclasite and in the hydrothermal quartz. The fault surface and associated preferred orientation zones were fragmented, offset and then cemented together with new hydrothermal quartz (Q_2) to form a second generation cataclasite (C_2).

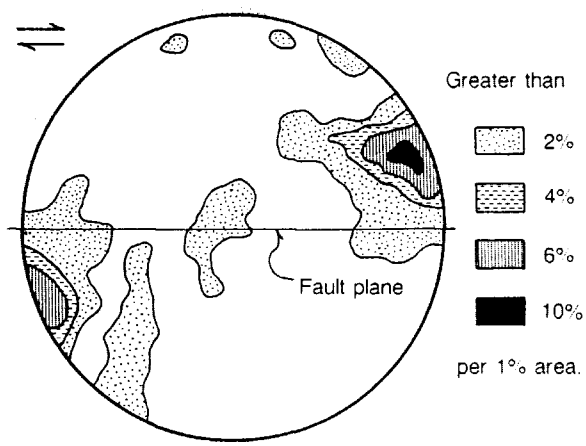

Fig. 8. c-Axis pole figure for the fine-grained slickenside surface material. The great circle represents the fault plane, with sense of slip shown at upper left. c-Axis data were measured using the photometric technique of Price (1980).

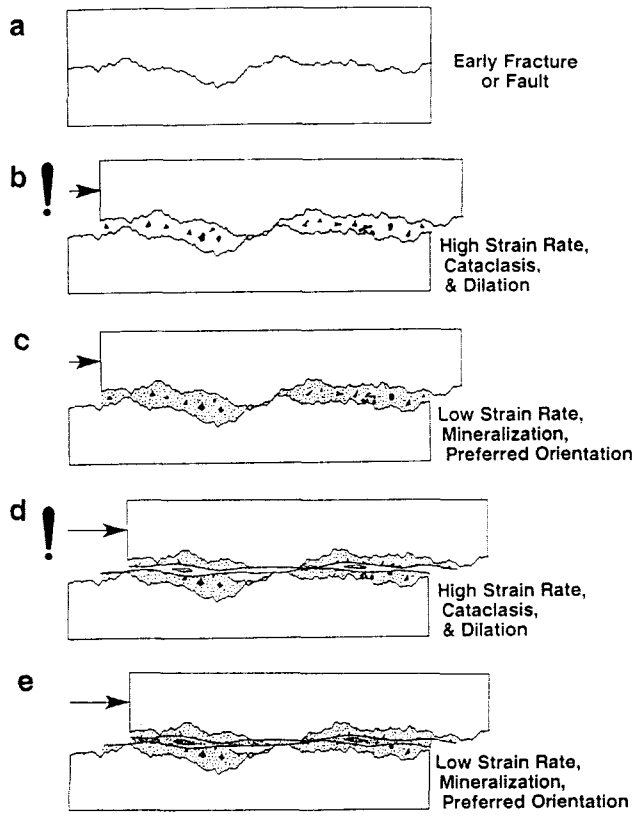

Fig. 10. Schematic diagrams illustrating the inferred development sequence for slickenside fault surfaces in Dixie Valley, Nevada. Alternating episodes of both discontinuous and continuous deformation are responsible for textural and mineralogic features preserved in the slickenside surface material and the cataclasite to either side of the surfaces. (a) We infer that the surface developed from pre-existing fracture or fault surfaces. (b) During seismic events, rapid translation of the surfaces relative to one another caused cataclasis and dilation along the fault surfaces. (c) Enhanced fluid flow after faulting resulted in the deposition of fine-grained hydrothermal quartz. Continued slow deformation caused the development of crystallographic preferred orientations. (d) and (e) Repeated episodes of cataclasis during seismic events, precipitation of hydrothermal minerals, and continuous deformation during the non-seismic phases of the earthquake cycle led to complex textures within the fault zone.

water pressure is equal to the lithostatic pressure (Hemley *et al.* 1980). If fluid pressure is less than the lithostatic pressure, or the fluid is not composed entirely of water, the reaction occurs at lower temperatures. The temperature estimate from the kaolinite plus quartz assemblage (less than 270°C) is consistent with the depth and temperature we inferred for slickenside formation from geologic constraints and geothermal investigations.

Transmission electron microscopy

The microstructure of the fine-grained quartz within the slickenside surface material is unusual. Examination by transmission electron microscopy (TEM) reveals that most of the grains are between 0.01 and 1.0 μm. Although the grains are approximately equant, they often have very irregular grain boundaries (Fig. 6b) and large surface areas. Smaller quartz grains and iron oxide grains are entirely included within larger quartz grains (Fig. 6c), a configuration of high surface energy. All the grains are essentially free of dislocations. Dislocations were rarely observed even after tilting and rotation of the ion-thinned specimens in the TEM. This microstructure is not typical of quartz which has been deformed within the dislocation creep field, nor of quartz which has been thermally annealed. The slickenside surface material contains no evidence for static grain growth or recrystallization. The samples shown in Figs. 6(a)–(c) were taken from the area with a strong crystallographic preferred orientation shown in Fig. 7(a).

In order to provide a contrast to the microstructure of the slickenside material, we include a TEM micrograph of a fine-grained quartz sample (novaculite) which was deformed experimentally in the dislocation creep field at 850°C, 1525 MPa confining pressure, a strain rate of 10^{-5} s^{-1} and to about 30% strain (Kronenberg & Tullis 1984). The sample (Fig. 6d) has undergone dynamic recrystallization and has straight grain boundaries, polygonal grains with approximately 120° grain junctions and a variable dislocation density. Annealing of this microstructure would only decrease the dislocation density and/or produce growth of new strain-free grains; the low energy configuration of the grain boundaries would be preserved. Thus the absence of dislocations and the presence of small grains with very irregular boundaries in the slickenside surface material is not consistent with deformation by dislocation creep or post-tectonic annealing.

Crystallographic preferred orientation

In many areas along the slickenside surfaces, a strong, optically visible, crystallographic preferred orientation is present in the fine-grained quartz material nearest the slickenside surface (Figs. 7a & b). The preferred orientation is usually confined to within 1–10 mm of the fault surfaces, and is most strongly developed along the smoother surfaces which have the greatest thickness of fine-grained quartz. Individual quartz grains within the area of preferred orientation are too fine-grained to measure crystallographic orientations with a U-stage, but the approximate location of the majority of *c*-axes in two dimensions was determined using a gypsum plate. The majority of *c*-axes are inclined in the direction of shear, and lie close to the plane perpendicular to the sliding surface which includes the sliding direction (Fig. 7b). Observations of one sample made with an X-ray pole figure device provide independent confirmation that the quartz has a crystallographic preferred orientation. Full *c*-axis pole figures were measured using the photometric technique of Price (1980). The computer reduction technique used in the photometric method assumes that individual quartz grains are as thick as the sample (7–20 μm). Because the slickenside surface material is extremely fine-grained (0.01–1 μm), this condition was not satisfied. This may cause the results to be slightly less accurate than would be obtained for coarser-grained materials. The results from the photometric technique (Fig. 8) confirm the conclusions obtained from optical observations using the gypsum plate; the *c*-axis pole figures showed single *c*-axis maxima. The orientations of the maxima are unusual, however, because they occur in the direction of extension, rather than in the direction of maximum shortening, as is often observed (Tullis *et al.* 1973, Schmid & Casey 1986).

Some of the slickensides display more complex patterns of preferred orientation (Figs. 7c & d) which are reminiscent of Riedel shear geometries described and interpreted by Logan *et al.* (1979). Features similar to both the shallowly inclined (R_1 type) and steeply inclined (R_2 type) Riedel shear zones are present. No evidence which precludes or demonstrates slip of the R_1 and R_2 zones was found. The *c*-axis orientations within the R_1 and R_2 zones, as determined with the gypsum plate, have the same relationship to the sense of shear inferred for R_1 and R_2 zones as is observed for the overall shear zone, namely the *c*-axes are inclined in the direction of shear (Figs. 7c & d).

Very similar crystallographic preferred orientations including Riedel shear geometries have been observed by Higgs (1981) in ultra fine-grained quartz (grain size <1 μm) deformed experimentally in shear at temperatures of 450 and 600°C, and shear strain rates of 10^{-2}–10^{-4} s^{-1}. The experiments which generated the preferred orientations were performed at confining pressures of 250 MPa and fluid (water) pressures of 100 MPa, while other experiments were performed at 150 MPa confining pressure with no water or fluid. Higgs observed some textural evidence of diffusive mass transfer (pressure solution) in the form of recrystallization and the formation of quartz veins in the wet experiments. Microscopic evidence for pressure solution or preferred orientation fabrics was not observed in the dry samples. Higgs offered no explanation for the development of the preferred orientation. Wenk & Kolòdny (1968) described preferred orientation in a fine-grained chert which probably formed as a result of deformation during diagenesis. They concluded that the preferred orien-

tation fabric they observed also must have formed at very low temperatures; the mechanism that produced the preferred orientations was unclear.

Interplay of continuous and discontinuous deformation

Outside the region of crystallographic preferred orientation, angular fragments in the cataclasite provide evidence of brittle deformation (Figs. 9a & b). The fragments range in size from 0.2 mm to larger than 10 cm, and include fragments of intact wallrock, fragments of earlier cataclasites, and of single crystal grains, usually quartz. The matrix between the angular fragments consists of randomly oriented, fine-grained quartz, which is texturally indistinguishable from the strongly oriented material which forms the slickenside surfaces.

Textural features of the slickenside surfaces provide clear evidence that cataclasis alternated with ductile deformation. Some of the angular fragments in the cataclasite are clearly derived from earlier fault surfaces which had crystallographic preferred orientations (Figs. 9a & b), providing evidence that conditions favorable for cataclasis alternated with conditions favorable for the development of preferred orientation. In some cases striking evidence of more than one cycle of alternating cataclastic and continuous deformation is well preserved (Figs. 9c & d). Stel (1981) described a similar history of alternating brittle failure, crystal growth and ductile deformation in cataclasites formed in granite rock.

None of the slickenside material we examined contains evidence for fiber growth either through the crack–seal mechanism (Ramsay 1980) or through pressure-solution slip (Elliott 1976). Some portions of the cataclasite to either side of the slickenside surfaces consist of dilation breccias with exploded-jigsaw textures, similar to those described by Sibson (1986b). Exploded-jigsaw texture means that angular cataclasite fragments appear as if they could be re-assembled if the intervening matrix material were removed. Sibson (1986b) inferred that exploded-jigsaw texture results from implosion brecciation, which is caused by the rapid opening of dilatant cavities along fault surfaces during seismic slip.

Figure 10 schematically illustrates the sequence of events which we believe caused the formation of the slickenside surfaces. The earliest history of the fault surfaces is difficult to ascertain (Fig. 10a). We presume the fault surfaces develop initially from either pre-existing fracture or fault surfaces. Textural features in the cataclasite (discussed above) indicate at least two phases of deformation were important in slickenside development. In the first phase (Fig. 10b) cataclasis and/or dilation between the surfaces caused the creation of new porosity, the disruption of pre-existing fault surfaces and the formation of angular fragments. The important elements of the second phase (Fig. 10c), include healing of the fault zone by the precipitation of new, hydrothermal quartz and the development of crystallographic preferred orientations. Precipitation of hydrothermal quartz may have been aided by enhanced fluid flow from seismically induced fluid pressure gradients (Nur & Booker 1972, Sibson *et al.* 1988), or from the development of marked disequilibrium between the fluid phase and the wallrock as a result of seismic faulting (Fournier 1985). Many repetitions of the two phases are responsible for the development of the slickenside surfaces (Figs. 10d & e).

DISCUSSION

Development of crystallographic preferred orientation in fine-grained quartz

Two features of the fine-grained quartz which forms the slickenside surfaces remain enigmatic. The first is the extremely fine-grained and non-equilibrium texture, and the second is the presence of crystallographic preferred orientation. In this section we discuss possible mechanisms for the development of these features. The preferred orientation and unique grain scale microstructure may have developed via a non steady-state mechanism. As we discuss above, it is quite possible that the fine-grained material which now forms the slickenside surfaces originally precipitated as ultra fine-grained amorphous silica, cristobalite or chalcedony. If the present microstructure developed from material of this type, a phase change and considerable grain coarsening must have occurred. If the preferred orientation developed during grain coarsening, or concurrently with a phase change, a steady-state mechanism would not have been responsible. Possible steady-state mechanisms include: (1) crystalline plasticity or dislocation creep; (2) strain alignment of sub-microscopic crystals; and (3) pressure solution. Although we favor pressure solution, a final conclusion as to which mechanism occurred is not possible, because few experimental studies have focused on exceedingly fine-grained quartz aggregates, because it is unclear whether the deformation was steady-state, and because it is unclear if important textural features of the slickenside material have been annealed or obliterated.

To place the conditions we infer for slickenside formation in context with relevant experimental data on deformation mechanisms, we show a plot of differential stress vs strain rate (Fig. 11). We can estimate the maximum differential stress during slickenside development because we know the depth at which the slickenside surfaces formed (2 km or less). Because Dixie Valley is characterized by normal faulting, we infer that the greatest principal compressive stress was vertical, and had a value consistent with a lithostatic pressure gradient (26 MPa km^{-1}) typical of average crustal rock densities (2.65 g cm^{-3}). The frictional strength of rock or Coulomb failure theory can be used to constrain the average total differential stress to 40 MPa or less (Brace & Kohlstedt 1980). Higher differential stresses may have been realized for short intervals during seismic events, or near asperities and irregularities in the fault zone. As mentioned earlier, strain rates during faulting may have varied from values as low as 10^{-15} s^{-1} or less

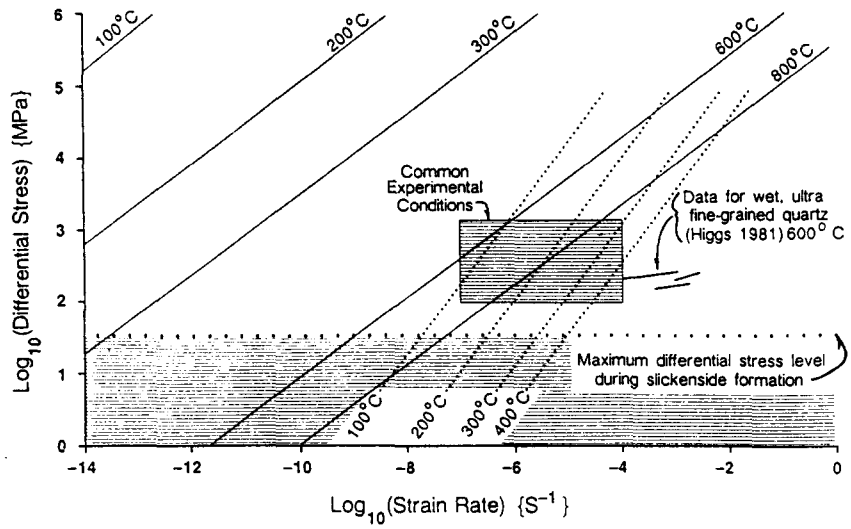

Fig. 11. Plot of differential stress vs strain rate, encompassing differential stress levels and strain rates for relevant experimental studies and for formation of natural slickenside surfaces. Differential stress levels and strain rates during slickenside formation in Dixie Valley are indicated by the shaded area below the heavy dotted line. Differential stress during slickenside formation can be constrained with knowledge of the depth of slickenside formation (less than 2 km—see text). Estimated strength of wet, coarse-grained (100 μm) quartz deforming by dislocation creep at different temperatures (solid lines) was calculated using equation (1) and the parameters given by Jaoul *et al.* (1984). Estimated strength of wet, fine-grained (1 μm) quartz deforming by pressure solution at different temperatures (fine dotted lines) was taken from Rutter (1983, fig. 10), and extrapolated to smaller grain size. Experiments on wet, ultra fine-grained quartz (grain size <1 μm) by Higgs (1981) were done at considerably higher strain rates than most experimental work. Recrystallization and the formation of aligned veins in Higgs samples suggests that some portion of their strain was accomplished by pressure solution. Extrapolation of stresses required for deformation by dislocation creep and by pressure solution suggest that at the conditions we infer for slickenside formation, pressure solution is more likely than dislocation creep.

(interseismic period) to values as high as 10^2 s^{-1} during seismic events.

Crystalline plasticity. The most common way that crystallographic preferred orientations develop is by slip of dislocations combined with material rotations required by continuity and the conservation of vorticity (Tullis *et al.* 1973, Lister *et al.* 1978, Schmid & Casey 1986). In a deforming aggregate, work hardening is prevented either by syntectonic recrystallization or by dislocation climb (Tullis & Yund 1985). Because both of these processes are thermally activated, dislocation creep is highly temperature sensitive. Based on extrapolation of laboratory data and study of naturally deformed rocks for which the temperatures during deformation can be well constrained, many studies have concluded that dislocation creep in quartz at typical geologic strain rates is only important at temperatures greater than about 300°C (Tullis *et al.* 1982, Sibson 1983, Simpson 1985). Flow laws for steady-state deformation of quartz (and many other minerals) typically have the form

$$\frac{d\varepsilon}{dt} = A\sigma^n e^{-(Q/RT)}, \quad (1)$$

where ε is strain, σ is differential stress, Q is an activation energy, T is temperature, R is the universal gas constant, and A and n are dimensionless constants (the 'pre-exponential term' and the stress exponent, respectively). Experimental results can be extrapolated to other temperatures and strain rates if the estimates of A, Q and n come from experiments which achieved steady-state conditions. Estimates of A, Q and n have been provided by Jaoul *et al.* (1984) for steady-state dislocation creep of coarse-grained quartzite (100 μm) in the presence of water (Fig. 11).

Extrapolation of predictions from Jaoul *et al.* (1984) to lower strain rates suggests that dislocation creep is an unlikely explanation for the development of crystallographic preferred orientations in the slickenside surface material in Dixie Valley, Nevada, because temperatures during slickenside formation were less than 270°C. Moreover, micron-scale textural features of the fine-grained surface material, most notably the complex grain-boundary geometries and the lack of visible dislocations, are inconsistent with deformation by dislocation motion. Additionally, the texture of the fine-grained quartz is not what would be expected for a fine-grained aggregate which first deformed by dislocation creep and then annealed statically. Both dislocation creep and static annealing mechanisms produce equigranular textures with simple, straight grain boundaries rather than the complex grain-boundary geometry observed in the slickenside surface material.

Strain alignment of sub-microscopic quartz grains. Another possibility for the development of crystallographic preferred orientations in the slickenside material is strain reorientation of rod-shaped crystals (Jeffery 1923, March 1932, reviewed by Tullis 1976 and Oertel 1985). The mechanism was originally proposed to explain the development of preferred orientation in quartz-rich metamorphic rocks by Sander (1930) and Schmidt (1932) (reviewed in Griggs & Bell 1938). In

order for a strain alignment mechanism to cause the development of preferred orientation in a quartz aggregate, individual grains must have non-equant shapes, the *c*-axes must be statistically aligned with one axis of the grains and grain-boundary sliding must be possible. Elongate, sub-microscopic quartz grains might form either by precipitation from an aqueous solution due to faster growth rates parallel to the *c*-axis, a possibility which we discuss below, or perhaps by comminution of pre-existing quartz grains. Although Griggs & Bell (1938) concluded that comminution of quartz grains produced fragments which are statistically elongate parallel to the *c*-axis, the dominant control on the orientation of the fragments in their experiments was the stress direction. In addition, Frondel (1962, pp. 104–109) and Dunning *et al.* (1984) both concluded that fracture and cleavage in quartz preferentially followed the *r* and *z* faces rather than the prism or *m* faces that would be required to create fragments elongated parallel to the *c*-axis. Because strain alignment could occur at very low temperatures, it is an attractive explanation for the formation of preferred orientation in the slickenside surface materials at Dixie Valley. Strain alignment seems unlikely, however, because there is no evidence of elongate quartz crystals in the Dixie Valley slickenside surface material (Figs. 6a–c).

Pressure solution. A third possibility for the development of crystallographic preferred orientation involves low-temperature crystallization of quartz directly from a fluid phase or colloid. Chalcedony, cristobalite, opal and other silica polymorphs are common in near surface hydrothermal deposits (Fournier 1985). These materials are particularly interesting for two reasons. First, these silica phases are very fine-grained, much like the slickenside surface material. Second, they often precipitate from supersaturated fluids that are in a state of disequilibrium with the wallrock, as seems to be the case in the Stillwater fault zone.

We suggest that crystallographic preferred orientations in fine-grained quartz may develop because of the tendency for quartz to grow and dissolve fastest in the direction parallel to the *c*-axis. The anisotropy in dissolution is easily demonstrated in strong acid (Meyer & Penfield 1889, Liang & Readey 1987), but we are not aware of completed experimental studies which document an anisotropy in water, although such studies are currently underway (H. Westrich, personal communication 1989). Preferred orientations in crack–seal veins of quartz (Cox & Etheridge 1983) are thought to be caused by crystallographically controlled anisotropy in crystal growth rates. Preferred orientations are also observed in fibrous chalcedony. Chalcedony fibers are usually aligned either parallel or perpendicular to the *c*-axes of the submicroscopic quartz that forms the fibers (Folk & Pittman 1971). Under experimental conditions, the orientation of the *c*-axes relative to the fiber axes can be controlled by changing the chemical environment (Oehler 1976, Kastner 1980). Precipitation of chalcedony with aligned *c*-axes has been observed experimentally at temperatures as low as 150–165°C (Oehler 1976, Kastner 1980). Because the crystallization of both quartz and chalcedony has been observed to form preferred orientations at low temperatures, we suggest a crystallization mechanism may explain the development of preferred orientation in the slickenside surface material from Dixie Valley. The question is, if crystallization and dissolution of quartz occurs simultaneously with strain of the rock, can a preferred orientation be produced that reflects the deformation?

In crack–seal or pressure-solution slip fibers, a preferred orientation of quartz can occur that reflects deformation and is due to precipitation from solution. Individual fibers in crack–seal veins or pressure-solution slickensides may have crystallographic orientations that are random, or that have the same crystallographic orientations as 'seed' crystals in the fracture walls (Durney & Ramsay 1973, Ramsay 1980, Cox & Etheridge 1983). In some cases, however, anisotropies in growth kinetics cause certain fiber orientations to be favored over others. This presumably occurs because fibers with their fast-growth directions essentially normal to the crack walls or parallel to the extension or opening direction impede or occlude fibers with other crystallographic orientations (Buckley 1951, pp. 262–263). Durney & Ramsay (1973, p. 73) and Spry (1969, p. 162) suggested that for quartz, fibers with their *c*-axes parallel to the fibers would predominate. Cox & Etheridge (1983) described two natural examples where the *c*-axes of crack–seal fibers had a small circle distribution with an opening angle of ~40°, which they attributed to preferential growth in the [1012] direction. Although this mechanism may explain preferred orientations in crack–seal veins and pressure-solution slip slickensides, it does not seem likely that the preferred orientation in the slickensides from the Stillwater fault zone is inherited from pressure-solution slip fibers, because no evidence of relict fibers was found in any of the fault zone materials.

Although it is unlikely that pressure-solution slip fibers existed on the slickensides from the Stillwater fault zone, it is possible that deformation by pressure solution in very fine-grained aggregates could produce a crystallographic preferred orientation of quartz by a similar process. As mentioned above, the rate of precipitation and dissolution in quartz depends on crystallographic orientation. We suggest that if the anisotropy is strong enough, crystallization and dissolution during pressure solution will depend on the orientations of the grain boundaries as well as the magnitude of stress across them, and that crystallographic preferred orientations might result. If the fastest growth direction in quartz is parallel to the *c*-axis, then grains with their *c*-axes oriented in the direction of extension should grow faster than grains of other orientations, whereas grains with their *c*-axes oriented in the direction of compression would undergo faster dissolution than others (Tullis 1989). One attraction of this mechanism as an explanation for the preferred orientations in the Dixie Valley slickensides is that it predicts that the *c*-axes should be oriented in the extension direction, as observed in the

slickenside surfaces (Figs. 7 and 8). One potential problem with this mechanism is that it should cause the development of elongate quartz grains, a feature which we did not observe.

Kamb (1959) used non-hydrostatic thermodynamics to develop a mechanism for the development of crystallographic preferred orientations during deformation by pressure solution. The driving force for solution transfer during pressure solution results from variations in normal stress across differently oriented grain boundaries. These normal stress variations cause variations in chemical potential. In Kamb's mechanism, small additional differences in chemical potential due to elastic anisotropy of the crystalline material are responsible for some grains growing at the expense of others. In the mechanism we propose above, the preferred orientation results from anisotropies in the kinetics of dissolution and growth, a different mechanism. To the best of our knowledge, there are no experimental or natural examples in which Kamb's mechanism has been shown to be responsible for an observed preferred orientation; the driving energy for this mechanism may be too small to be important. Kamb's predicted patterns of preferred orientation do not match those we observe, although, as discussed by Paterson (1973), the predictions of Kamb's model can be quite dependent on details of the processes that are allowed to operate.

As discussed above, Higgs (1981) has performed a set of experiments on ultra fine-grained quartz (grain size $<1\ \mu m$), both with excess water and dry. In the wet experiments, Higgs observed both preferred orientations and evidence of pressure solution or diffusive mass transfer. Microscopic evidence for pressure solution or preferred orientation fabrics was not observed in the dry samples. Higgs observed that the wet samples were considerably weaker than the dry samples, suggesting that different deformation mechanisms contributed to the strain in the wet and dry experiments. The combination of the textural evidence, the change in mechanical behavior in the presence of water, and the lower strength of the ultra fine-grained quartz relative to coarser-grained material suggests that the mechanism of pressure solution was active. Because Higgs (1981) observed preferred orientations that are very similar to those observed in the slickenside surface material from Dixie Valley, Nevada, we suggest that the same mechanism is responsible for the preferred orientation in both the experimental and natural cases, and that this mechanism involves both pressure solution and a growth/dissolution rate anisotropy in quartz, as discussed above.

Unfortunately, the mechanical data from the study by Higgs (1981) do not allow accurate estimates of the stress exponent or the activation energy, precluding extrapolation of the observed strengths to lower strain rates and temperatures. Estimates of the strength of quartz aggregates deforming by pressure solution have been provided by Rutter (1983). Figure 11 shows Rutter's predictions, which were extrapolated to a grain size of $1\ \mu m$ using an inverse cubic dependence of strain rate on grain size (Rutter 1983, equation 4). Rutter's predictions, the results of Higgs' experiments, and the predictions from extrapolation of dislocation creep flow laws (Fig. 11) suggest that for the slickenside surface material deformation by pressure solution is more likely than deformation by dislocation creep. The results of Higgs' (1981) experimental study, coupled with the observations reported in this study, suggest that additional experimental work on fine-grained quartz aggregates would be worthwhile.

Summary. We cannot argue conclusively for a single explanation for the development of the crystallographic preferred orientation in the fine-grained slickenside surface material. Crystalline plasticity is an unlikely mechanism because the temperatures we infer for slickenside formation seem too low and because the extreme variation in grain size, the complex grain-boundary geometries, and the extremely low dislocation density observed in the slickenside surface material are inconsistent with dislocation motion. Strain alignment of submicroscopic quartz fragments elongate in the *c*-axis direction seems unlikely, because the texture of the fine-grained slickenside material shows no elongate grains. Crystallographic preferred orientation in the slickenside material is probably not inherited from pressure-solution slip fibers, because relict fibers were not found in any of the slickenside surface materials. It seems most likely that a mechanism associated with pressure solution and the growth/dissolution rate anisotropy of quartz caused the preferred orientations in the slickenside material.

CONCLUSIONS

Slickenside surfaces along the Stillwater fault zone in the Dixie Valley area of Central Nevada, U.S.A., formed at depths of less than about 2 km and temperatures that were less than 270°C. The slickenside surface material is composed of very fine-grained ($0.01–1.0\ \mu m$) quartz with small amounts of iron oxide and kaolinite. Evidence of both continuous and discontinuous deformation processes are present in the slickenside surface material, and textural features in the slickenside surface material indicate that the continuous and discontinous processes alternated in time. Because the crystallographic preferred orientation is probably related to strain, and probably developed at relatively low strain rates, we correlate the continuous deformation phase of slickenside formation with the low-strain-rate phases of the earthquake cycle. We tentatively correlate the discontinuous deformation phase characterized by cataclasis with the higher-strain-rate, seismic portion of the earthquake cycle. The wide range of strain rates which occur during the seismic cycle may be an essential element in the formation of fine-grained, glassy slickensides observed at Dixie Valley, Nevada, and many other areas.

Acknowledgements—We wish to express special thanks to Dick Yund for electron microscope work, Maura Weathers for X-ray observations, and Paul Williams for measuring quartz *c*-axis preferred orientations. Dick Yund, Bill Parry, Fred Chester, Greg Hirth, Jan Tullis and Tim Byrne provided helpful comments and suggestions. Tim Byrne, Mike Blanpied, Melissa Huther and Eileen Brennan provided indispensable assistance in the field. This work was supported by National Science Foundation grants EAR-8509014 and EAR-8610088.

REFERENCES

Anderson, R. E., Zoback, M. L. & Thompson, G. A. 1983. Implications of selected subsurface data on the structural form and evolution of some basins in the northern Basin and Range province, Nevada and Utah. *Bull. geol. Soc. Am.* **94**, 1055–1072.

Angelier, J. 1979. Determination of the mean principal directions of stresses for a given fault population. *Tectonophysics* **56**, T17–T26.

Angelier, J., Colletta, B. & Anderson, R. E. 1985. Neogene paleostress changes in the Basin and Range: a case study at Hoover Dam, Nevada–Arizona. *Bull. geol. Soc. Am.* **96**, 347–361.

Avakian, A. J. 1986. Mirror-quality polished fault surfaces from the Last Chance Range, East-Central California. *Geol. Soc. Am. Abs. w. Prog.* **18**, 530.

Brace, W. F. & Kohlstedt, D. L. 1980. Limits on lithospheric stress imposed by laboratory experiments. *J. geophys. Res.* **85**, 6248–6252.

Brune, J. 1976. The physics of earthquake strong motion. In: *Seismic Risk and Engineering Decision* (edited by Lomnitz, C. & Rosenblueth, E.). Elsevier, Amsterdam, 141–177.

Buckley, H. E. 1951. *Crystal Growth*. John Wiley, New York.

Burford, R. O. & Harsh, P. W. 1980. Slip on the San Andreas fault in central California from alignment array surveys. *Bull. seism. Soc. Am.* **70**, 1233–1261.

Cox, S. F. & Etheridge, M. A. 1983. Crack–seal fibre growth mechanisms and their significance in the development of oriented layer silicate microstructures. *Tectonophysics* **92**, 147–170.

Denton, J. M., Bell, E. J. & Jodry, R. L. 1980. Geothermal reservoir assessment case study: northern Dixie Valley, Nevada. Southland Royalty Co., Fort Worth, Texas, U.S.A.

Dozer, D. I. 1986. Earthquake processes in the Rainbow Mountain–Fairview Peak–Dixie Valley, Nevada, Region 1954–1959. *J. geophys. Res.* **91**, 12572–12586.

Dunning, J. D., Schuyler, J. & Owens, A. 1984. The effects of aqueous chemical environments on crack propagation in quartz. *J. geophys. Res.* **89**, 4115–4123.

Durney, D. W. & Ramsay, J. G. 1973. Incremental strains measured by syntectonic crystal growths. In: *Gravity and Tectonics* (edited by DeJong, K. A. & Scholten, R.). John Wiley, New York, 67–96.

Elliott, D., 1976. The energy balance and deformation mechanisms of thrust sheets. *Phil. Trans. R. Soc. Lond.* **A283**, 289–312.

Engelder, J. T. 1974. Microscopic wear grooves on slickensides: indicators of paleoseismicity. *J. geophys. Res.* **79**, 4387–4392.

Fleuty, M. J. 1975. Slickensides and slickenlines. *Geol. Mag.* **112**, 319–322.

Folk, R. L. & Pittman, J. S. 1971. Length-slow chalcedony: a new testament for vanished evaporites. *J. sedim. Petrol.* **41**, 1045–1058.

Fonseca, J. 1988. The Sou Hills: a barrier to faulting in the Central Nevada Seismic Belt. *J. geophys. Res.* **93**, 475–489.

Fournier, R. O. 1985. The behavior of silica in hydrothermal solutions. In: *Geology and Geochemistry of Epithermal Systems* (edited by Berger, B. R. & Bethke, P. M.). *Rev. Econ. Geol.* **2**, 45–59.

Frondel, C. 1962. *The System of Mineralogy, Volume* III. *Silica Minerals*. John Wiley, New York.

Gray, M. B. & Nickelsen, R. P. 1989. Pedogenic slickensides, indicators of strain and deformation processes in redbed sequences of the Appalachian foreland. *Geology* **17**, 72–75.

Griggs, D. & Bell, J. F. 1938. Experiments bearing on the orientation of quartz in deformed rocks. *Bull. geol. Soc. Am.* **49**, 1723–1746.

Hancock, P. L. & Barka, A. A. 1987. Kinematic indicators on active normal faults in Western Turkey. *J. Struct. Geol.* **9**, 573–584,

Hastings, D. D. 1979. Results of exploratory drilling, northern Fallon Basin, western Nevada. In: *Basin and Range Symposium* (edited by Newman, G. W. & Good, H. D.). *Rocky Mountain Ass. Geol.–Utah Geol. Ass*, Denver, Colorado, 515–522.

Hemley, J. J., Montoya, J. W., Marinenko, J. W. & Luce, R. W. 1980. Equilibria in the system Al_2O_3–SiO_2–H_2O and some general implications for alteration/mineralization processes. *Econ. Geol.* **75**, 210–228.

Higgs, N. G. 1981. Mechanical properties of ultrafine quartz, chlorite and bentonite in environments appropriate to upper-crustal earthquakes. Unpublished Ph.D. thesis, Texas A&M University, College Station, Texas, U.S.A.

Jaoul, O., Tullis, J. & Kronenberg, A. 1984. The effect of varying water contents on the creep behavior of Heavitree Quartzite. *J. geophys. Res.* **89**, 4298–4312.

Jeffery, G. B. 1923. The motion of ellipsoidal particles immersed in a viscous fluid. *Proc. R. Soc. Lond.* **A102**, 161–179.

Kamb, W. B. 1959. Theory of preferred crystal orientation developed by crystallization under stress. *J. Geol.* **67**, 153–170.

Kastner, M. 1980. Length-slow chalcedony: the end of the new testament. *Eos, Trans. Am. Geophys. Un.* **61**, 399.

Kronenberg, A. K. & Tullis, J. 1984. Flow strengths of quartz aggregates: grain size and pressure effects due to hydrolytic weakening. *J. geophys. Res.* **89**, 4281–4297.

Lachenbruch, A. H. & Sass, J. H. 1977. Heat flow in the United States and the thermal regime of the crust. In: *The Earth's Crust* (edited by Heacock, J. G.). *Am. Geophys. Un. Washington, DC*, 626–675.

Liang, D.-T. & Readey, D. E. 1987. Dissolution kinetics of crystalline and amorphous silica in hydrofluoric–hydrochloric acid mixtures. *J. Am. Ceram. Soc.* **70**, 570–577.

Lister, G. S., Paterson, M. S. & Hobbs, B. E. 1978. The simulation of fabric development in plastic deformation and its application to quartzite: the model. *Tectonophysics* **45**, 107–158.

Logan, J. M., Friedman, M., Higgs, N., Dengo, C. & Shimamoto, T. 1979. Experimental studies of simulated fault gouge and their application to studies of natural fault zones. *U.S. Geol. Surv. Open-File Rep.* **79-1239**, 305–343.

March, A. 1932. Mathematische theorie der regelung nach der korngestalt bei affiner deformation. *Z. Kristallogr.* **81**, 285–298.

Means, W. D. 1987. A newly recognized type of slickenside striation. *J. Struct. Geol.* **9**, 585–590.

Meyer, O. & Penfield, S. L. 1889. Results obtained by etching a sphere and crystals of quartz with hydrofluoric acid. *Trans. Conn. Acad.* **8**, 158–165.

Nur, A. & Booker, J. R. 1972. Aftershocks caused by pore fluid flow? *Science* **175**, 885–887.

Oehler, J. H. 1976. Hydrothermal crystallization of silica gel. *Bull. geol. Soc. Am.* **87**, 1143–1152.

Oertel, G. 1985. Reorientation due to grain shape. In: *Preferred Orientation in Deformed Metals and Rocks: An Introduction to Modern Texture Analysis* (edited by Wenk, H.-R.). Academic Press, New York, 259–265.

Okaya, D. A. & Thompson, G. A. 1985. Geometry of Cenozoic extensional faulting: Dixie Valley, Nevada. *Tectonics* **4**, 107–125.

Page, B. M. 1965. Preliminary geologic map of a part of the Stillwater Range, Churchill County, Nevada. Map 28, Nevada Bureau of Mines and Geology, Reno, Nevada, U.S.A.

Parchman, W. L. & Knox, J. W. 1981. Exploration for geothermal resources in Dixie Valley, Nevada. *Bull. Geotherm. Resources Council* **10**, 3–6.

Paterson, M. S. 1973. Nonhydrostatic thermodynamics and its geologic applications. *Rev. Geophys. & Space Phys.* **11**, 355–389.

Petit, J. P. 1987. Criteria for the sense of movement on fault surfaces in brittle rocks. *J. Struct. Geol.* **9**, 597–608.

Pfiffner, O. A. & Ramsay, J. G. 1982. Constraints on geological strain rates: arguments from finite strain states of naturally deformed rocks. *J. geophys. Res.* **87**, 311–321.

Power, W. L., Tullis, T. E., Brown, S. R., Boitnott, G. N. & Scholz, C. H. 1987. Roughness of natural fault surfaces. *Geophys. Res. Lett.* **14**, 29–32.

Power, W. L., Tullis, T. E. & Weeks, J. D. 1988. Roughness and wear during brittle faulting. *J. geophys. Res.* **93**, 15,268–15,278.

Price, G. P. 1980. The analysis of quartz *c*-axis fabrics by the photometric method. *J. Geol.* **88**, 181–195.

Ramsay, J. G. 1980. The crack–seal mechanism of rock deformation. *Nature* **284**, 135–139.

Riehle, J. R., McKee, E. H. & Speed, R. C. 1972. Tertiary volcanic center, west-central Nevada. *Bull. geol. Soc. Am.* **83**, 1383–1396.

Rutter, E. H. 1983. Pressure solution in nature, theory and experiment. *J. geol. Soc. Lond.* **140**, 725–240.

Sander, B. 1930. *Gefugekunde der Gesteine*. Springer, Wien.

Schmid, S. M. & Casey, M. 1986. Complete fabric analysis of some commonly observed quartz *c*-axis patterns. In: *Mineral and Rock Deformation: Laboratory Studies* (edited by Hobbs, B. E. & Heard, H. C.). *Am. Geophys. Un. Geophys. Monogr.* **36**, 263–286.

Schmidt, W. 1932. *Tektonik und Verformungslehre.* Geb. Borntraeger, Berlin.
Sibson, R. H. 1975. Generation of pseudotachylyte by ancient seismic faulting. *Geophys. J. R. astr. Soc.* **43**, 775–794.
Sibson, R. H. 1977. Fault rocks and fault mechanisms. *J. geol. Soc. Lond.* **133**, 191–231.
Sibson, R. H. 1983. Continental fault structure and the shallow earthquake source. *J. geol. Soc. Lond.* **140**, 741–767.
Sibson, R. H. 1986a. Earthquakes and lineament infrastructure. *Phil. Trans. R. Soc. Lond.* **A317**, 63–79.
Sibson, R. H. 1986b. Brecciation processes in fault zones: inferences from earthquake rupturing. *Pure & Appl. Geophys.* **124**, 159–175.
Sibson, R. H., Robert, F. & Poulsen, K. H. 1988. High-angle reverse faults, fluid pressure cycling, and mesothermal gold–quartz deposits. *Geology* **16**, 551–555.
Simpson, C. 1985. Deformation of granitic rocks across the brittle–ductile transition. *J. Struct. Geol.* **7**, 503–511.
Spry, A. 1969. *Metamorphic Textures.* Pergamon, London.
Stel, H. 1981. Crystal growth in cataclasites: diagnostic microstructures and implications. *Tectonophysics* **78**, 585–600.
Thatcher, W. 1979. Systematic inversion of geodetic data in central California. *J. geophys. Res.* **84**, 2283–2295.
Thompson, G. A. & Burke, D. B. 1973. Rate and direction of spreading in Dixie Valley, Basin and Range province, Nevada. *Bull. geol. Soc. Am.* **84**, 627–632.
Tjia, H. D. 1968. Fault-plane markings. *XXIII Int. Geol. Congr.* **13**, 279–284.
Tullis, T. E. 1976. Experiments on the origin of slaty cleavage and schistosity. *Bull. geol. Soc. Am.* **87**, 745–753.
Tullis, T. E. 1989. Development of preferred orientation due to anisotropic dissolution/growth rates during solution-transfer creep. *EOS, Trans. Am. Geophys. Un.* **70**, 457–458.
Tullis, J., Christie, J. M. & Griggs, D. T. 1973. Microstructures and preferred orientations of experimentally deformed quartzites. *Bull. geol. Soc. Am.* **84**, 297–314.
Tullis, J., Snoke, A. W. & Todd, V. R. 1982. Significance and petrogenesis of mylonitic rocks. *Geology* **10**, 227–230.
Tullis, J. & Yund, R. A. 1985. Dynamic recrystallization of feldspar: a mechanism for ductile shear zone formation. *Geology* **13**, 238–241.
Wallace, R. E. & Whitney, R. A. 1984. Late Quaternary history of the Stillwater Seismic Gap, Nevada. *Bull. seism. Soc. Am.* **74**, 301–314.
Wenk, H. R. & Kolodny, Y. 1968. Preferred orientation of quartz in a chert breccia. *Proc. natn. Acad. Sci. U.S.A.* **59**, 1061–1066.
Will, T. M. & Wilson, C. J. L. 1989. Experimentally produced slickenside lineations in pyrophyllitic clay. *J. Struct. Geol.* **11**, 657–667.
Wojtal, S. 1986. Deformation within foreland thrust sheets by populations of minor faults. *J. Struct. Geol.* **8**, 341–360.
Zoback, M. L. 1989. State of stress and modern deformation of the northern Basin and Range province. *J. geophys. Res.* **94**, 7105–7128.